The transient appearance of zipper-like actin superstructures during the fusion of osteoclasts

Jiro Takito[1,*], Masanori Nakamura[2], Masaki Yoda[1], Takahide Tohmonda[1], Shinichi Uchikawa[1], Keisuke Horiuchi[1], Yoshiaki Toyama[1] and Kazuhiro Chiba[1,*]

[1]Department of Orthopedic Surgery, School of Medicine, Keio University, Tokyo, Japan
[2]Department of Oral Anatomy and Developmental Biology, School of Dentistry, Showa University, Tokyo, Japan
*Authors for correspondence (takito@sc.itc.keio.ac.jp; kchiba@sc.itc.keio.ac.jp)

Accepted 11 November 2011
Journal of Cell Science 125, 662–672

doi: 10.1242/jcs.090886

Summary

Multinucleated osteoclasts are responsible for bone resorption. Hypermultinucleated osteoclasts are often observed in some bone-related diseases such as Paget's disease and cherubism. The cellular mechanics controlling the size of osteoclasts is poorly understood. We introduced EGFP–actin into RAW 264.7 cells to monitor actin dynamics during osteoclast differentiation. Before their terminal differentiation into osteoclasts, syncytia displayed two main types of actin assembly, podosome clusters and clusters of zipper-like structures. The zipper-like structures morphologically resembled the adhesion zippers found at the initial stage of cell–cell adhesion in keratinocytes. In the zipper-like structure, Arp3 and cortactin overlapped with the distribution of dense F-actin, whereas integrin β3, paxillin and vinculin were localized to the periphery of the structure. The structure was negative for WGA–lectin staining and biotin labeling. The zipper-like structure broke down and transformed into a large actin ring, called a podosome belt. Syncytia containing clusters of zipper-like structures had more nuclei than those with podosome clusters. Differentiated osteoclasts with a podosome belt also formed the zipper-like structure at the cell contact site during cell fusion. The breakdown of the cell contact site resulted in the fusion of the podosome belts following plasma membrane fusion. Additionally, osteoclasts in mouse calvariae formed the zipper-like structure in the sealing zone. Therefore, we propose that the zipper-like actin superstructures might be involved in cell–cell interaction to achieve efficient multinucleation of osteoclasts. Understanding of the zipper-like structure might lead to selective therapeutics for bone diseases caused by hypermultinucleated osteoclasts.

Key words: Osteoclast, Multinucleation, Actin, Podosome

Introduction

Osteoclasts differentiate from monocyte and/or macrophage lineage cells in response to macrophage colony-stimulating factor (M-CSF) and receptor activator of NF-κB ligand (RANKL; also known as tumor necrosis factor ligand superfamily member 11) (Suda et al., 1999). The fusion of mononuclear precursor cells produces multinucleated cells (Vignery, 2005; Helming and Gordon, 2009). Multinucleation enhances the resorbing efficiency of osteoclasts both in vivo and in vitro (Yagi et al., 2005).

Aberration of multinucleation or size control of osteoclasts is seen in some bone diseases. Paget's disease is characterized by localized areas of increased bone resorption coupled with exuberant new bone formation with primary cellular abnormality of osteoclasts (Roodman and Windle, 2005). Although normal human osteoclasts in the bone contain three to ten nuclei per cell, pagetic osteoclasts contain up to 100 nuclei. Osteoclasts differentiated from human and mouse bone marrow cells overexpressing measles virus nucleocapsid protein (MVNP) gene, a causative gene for Paget's disease, contain more nuclei than the control osteoclasts (Kurihara et al., 2000; Kurihara et al., 2011). Cherubism is a dominantly inherited syndrome characterized by excessive bone resorption in the jaws and accumulation of inflammatory and/or fibrous tissue in the lower face. Osteoclasts differentiated from bone marrow cells obtained from homozygous cherubism knockin mice carrying a proline to arginine mutation (P416A) in the SH3-binding adaptor protein, SH3BP3, contain ~60 nuclei per cell (Ueki et al., 2007). These observations suggest that osteoclasts have a cell autonomous mechanism to regulate their size. Signals from the environment also induce giant osteoclasts (Bozec et al., 2008). The long bones of newborn mice deficient for the Fos-related protein Fra-2 have giant osteoclasts. In this case, giant osteoclast induction is caused by placental hypoxia mediated by a pathway involving leukemia inhibitory factor (LIF), prolyl hydroxylase 2 (PHD2), hypoxia-induced factor 1α (HIF1α) and Bcl2.

In vitro osteoclastogenesis induced by M-CSF and RANKL produces large osteoclasts that contain ~100 nuclei, and have a diameter of over 1 mm. Therefore, elucidation of the cellular mechanism of giant osteoclast formation in vitro might shed light on the etiology of the disease-related hypermultinucleated osteoclasts described above. Because cell shape is regulated by reorganization of the actin cytoskeleton (Hall, 1998), we focused our investigations on the changes of actin filament structures in the multinucleation process during osteoclastogenesis. In osteoclasts, various actin assemblies found in the ventral membranes attach to the extracellular matrix or bone. The structural unit of such variation is believed to be a podosome, an actin-rich membrane-spanning superstructure (Jurdic et al., 2006; Spinardi and Marchisio, 2006). Podosomes are composed of a

Journal of Cell Science

dense F-actin core surrounded by an unpolymerized actin cloud containing integrin receptors. The function of podosomes is believed to be cell–matrix adhesion, matrix degradation and tissue invasion (Larsen et al., 2006; Linder, 2007). The turnover rate of podosome is ~2 minutes (Destaing et al., 2003). Reorganization of podosomes involves the formation of a small ring, called a podosome ring. Podosome rings also have a rapid turnover and occupy only a part of the ventral membrane in immature osteoclasts. Fusion of podosome rings results in a podosome belt that demarcates the cell periphery of differentiated osteoclasts on glass (Kanehisa et al., 1990). A podosome belt covers almost the whole ventral membrane and is stable over several hours.

Cell fusion includes a stage of adhesion between mononuclear precursor cells before membrane fusion (Vignery, 2005; Helming and Gordon, 2009). This coincides with the results that plating cell density affects the size and morphology of in-vitro-differentiated osteoclasts (Gardner, 2007). A cell–cell adhesion molecule E-cadherin is reported to be involved in the fusion of mononuclear precursor cells during osteoclastogenesis (Mbalaviele et al., 1995). It is known that reorganization of the actin cytoskeleton is needed for the recruitment of E-cadherin at the cell contact site (Cavey and Lecuit, 2009). In the initial stage of adherens junction formation, keratinocytes exhibit a conspicuous actin superstructure termed the adhesion zipper, in which actin bundles run perpendicularly to the axis of the cell contact area and link two cells together (Vasioukhin et al., 2000). Similar actin superstructures are also observed in simple epithelia (Adams et al., 1998) and fibroblasts (Gloushankova et al., 1998). So, a question arises whether osteoclast precursors form a similar actin-based adhesion structure during multinucleation. Here, we report that the murine macrophage cell line RAW 264.7 when plated on glass transiently expresses a zipper-like superstructure during differentiation into osteoclasts. Similar zipper-like structures are also found in osteoclasts derived from mouse bone marrow macrophages grown on a dentine slice, and in osteoclasts in mouse calvariae. We propose that this actin-based superstructure is involved in osteoclast hypermultinucleation.

Results

F-actin structures in mononuclear cells before cell fusion

To detect the reorganization of F-actin during differentiation into osteoclasts, we plated RAW 264.7 cells on glass coverslips and stained them with Rhodamine–phalloidin. RAW 264.7 cells, a cell line that is widely used for studies of osteoclast differentiation, become osteoclasts within 4 days of stimulation with RANKL. All mononuclear cells had podosomes in their ventral membrane 1 day after RANKL stimulation (Fig. 1A). A small proportion of mononuclear cells had asymmetrically localized actin rings (circular actin superstructures; Fig. 1B). At 3 days after RANKL addition, RAW264.7 cells formed cell aggregates. Some cells in the aggregate possessed podosome clusters, whereas others had actin rings at the bottom of cells (Fig. 1C). In a third case, the actin distribution was columnar, similar to that found in epithelia (Fig. 1C,D).

Zipper-like F-actin superstructures in the syncytium

At 3 days after RANKL stimulation, many syncytia can be observed. To detect the plasma membrane of syncytia, we used wheat germ agglutinin (WGA)–lectin, which recognizes *N*-acetylglucosamine and terminal neuraminic acid (Nagata and

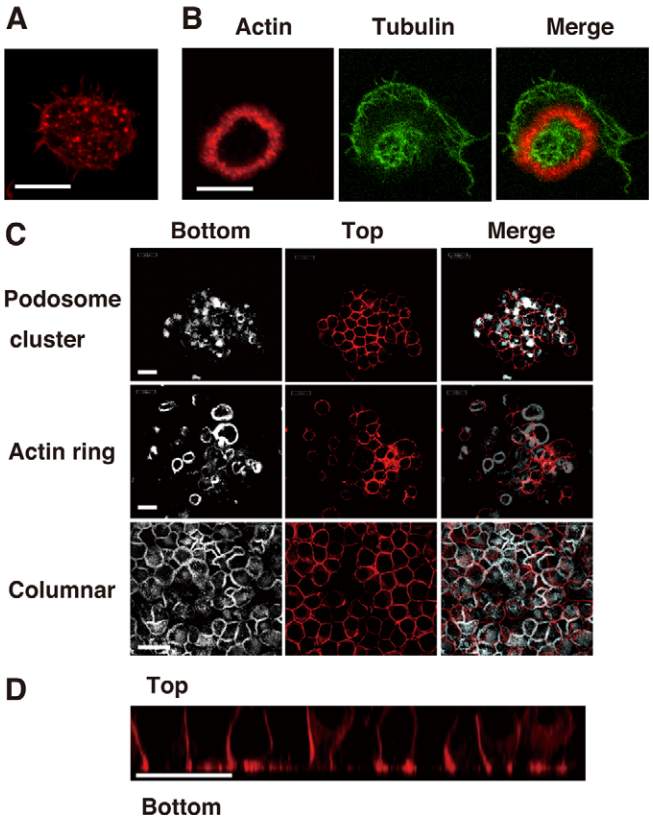

Fig. 1. Variations in F-actin superstructures in mononuclear cells and cell aggregates. (**A**) A mononuclear cell with podosomes. On day 1 after the addition of RANKL, RAW 264.7 cells were fixed and stained with Rhodamine–phalloidin. Scale bar: 10 μm. (**B**) A mononuclear cell with an actin ring. On day 1 after the addition of RANKL, RAW 264.7 cells were fixed and stained with Rhodamine–phalloidin and anti-tubulin antibody. Note that the actin ring occupied only a part of the ventral membrane. Scale bar: 10 μm. (**C**) The diversity of actin superstructures in the ventral membranes of cell aggregates. Cell aggregates with podosome clusters at their ventral membrane (upper row), with actin rings at their ventral membrane (central row) and with a columnar cytoskeleton (lower row). On day 3 after the addition of RANKL, RAW 264.7 cells were fixed and stained with Rhodamine–phalloidin. Confocal images were taken of the bottom (left column) and the top of the aggregate (center column). The images were merged to allow comparison the actin cytoskeletons at the two sites. The bottom images of the aggregates show the diversity of actin structures. Scale bars: 20 μm. (**D**) Z-section of the cell aggregates showing the columnar cytoskeleton. Scale bar: 20 μm.

Burger, 1974). WGA–lectin heavily stained the dorsal part of the plasma membrane of osteoclasts (Illes and Fischer, 1989; Salo et al., 1996) but it also stained other parts of the membrane. WGA–lectin staining showed that fusion of the plasma membranes of syncytia occurred in the dorsal domain first (Fig. 2A). The syncytia contained many nuclei, which were located in the center of the cell, and microtubules ran from the center to the cell periphery (Fig. 2B). Hence, syncytia probably represent one of the intermediate states produced after membrane fusion between mononuclear cells. One type of syncytium had podosome clusters in its ventral membrane, whereas another had a cluster of actin rings. The latter was frequently found in areas of high cell density on the glass coverslip. The cluster of actin rings covered the whole ventral membrane. Each actin ring had many

contact sites with others and formed a zipper-like structure at each contact site (Fig. 2C). The number of actin rings per syncytium ranged from three to 20. The zipper-like structure spanned 5~10 μm in width, varied in length, and extended 1 μm from the bottom of the cell. The morphology of this actin superstructure was quite different from those of podosomes, podosome rings and the podosome belt (Fig. 2D). Because the superstructure resembles the adhesion zipper in keratinocytes (Vasioukhin et al., 2000), we tentatively called it the zipper-like structure. The presence of the zipper-like structure in a more physiological context was tested with osteoclasts derived from bone marrow macrophages seeded onto a dentine slice. As shown in Fig. 2E, osteoclasts derived from bone marrow macrophages of ddY, C57BL and ICR mice also exhibited the cluster of actin rings when treated this way. The contact site of actin rings in these cells also formed the zipper-like structure.

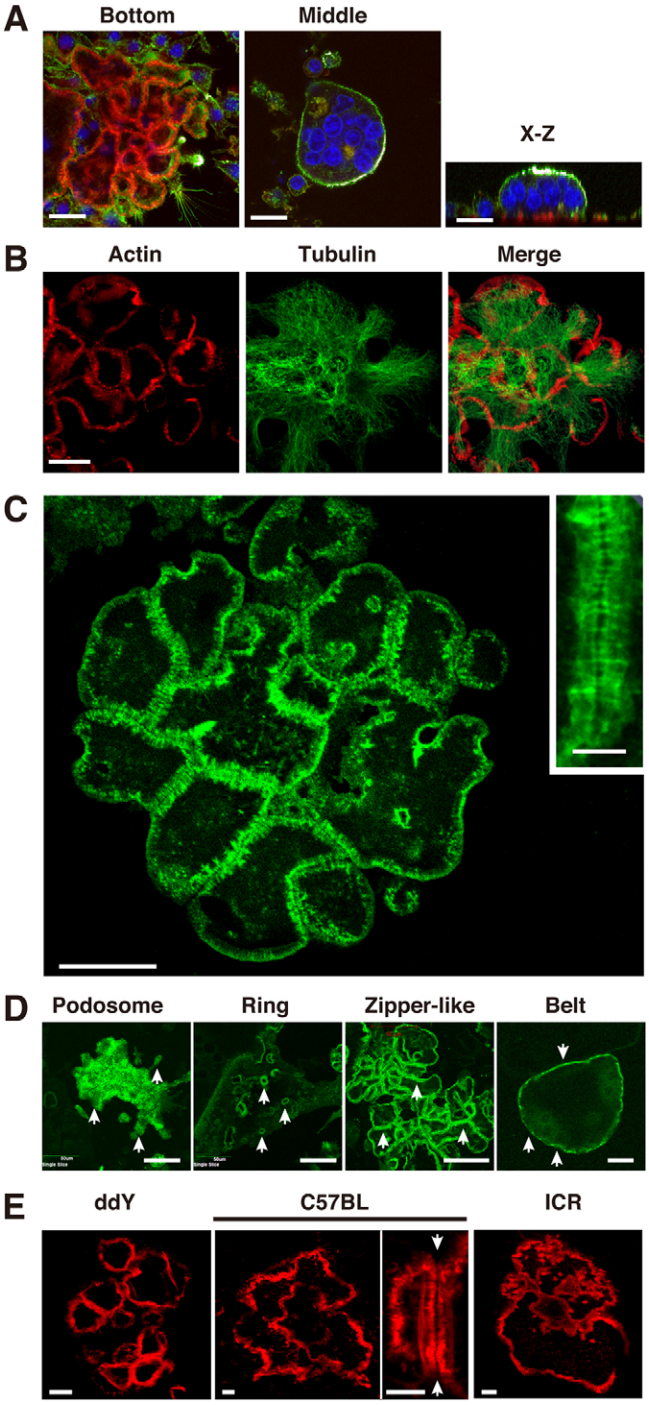

Protein components of the zipper-like structure

We examined the localization of protein components of the podosome in the zipper-like structure by confocal microscopy. A dense F-actin core of the podosome contains proteins necessary for polymerization and depolymerization of actin filaments, such as Arp2/3 and cortactin (Jurdic et al., 2006; Spinardi and Marchisio, 2006). The core is surrounded by an unpolymerized actin cloud containing podosome adhesion-mediating proteins such as integrin αvβ3, vinculin and paxillin. Arp3 and cortactin overlapped with the thick distribution of actin in the zipper-like structure (Fig. 3A,B). By contrast, integrin β3, vinculin and paxillin were localized at the outer edge of the zipper-like structure (Fig. 3C–E). The results suggest that the zipper-like structure has similar molecular components to the podosome and the podosome belt. These actin superstructures all have a central actin core that is surrounded by the integrin-based adhesion structure.

We wondered whether the zipper-like structure contains the cell–cell adhesion molecules that characterize the adherens junctions of epithelia. The zipper-like structure was negative for E-cadherin and β-catenin staining that is observed in epithelia. However, we could not eliminate the possibility that very small amounts of these two molecules are contained in the zipper-like structure. Epithelia utilize another pair of cell-cell adhesion molecules, afadin and nectin (Takai et al., 2008). Afadin colocalizes with the F-actin core of the zipper-like superstructure in syncytia (Fig. 3F). Afadin is reported to localize in the podosomes of A7r5 smooth muscle cells (Kremerskothen et al., 2011). Surprisingly, a tight junction protein, zonula occludens 1 (ZO-1), has also been shown to act as a component of podosomes in human macrophages and human osteoclasts. These observations support the notion that the zipper-like structure is involved in adhesion in the ventral membrane of a syncytium.

Fig. 2. Some syncytia contain zipper-like actin superstructures during osteoclastogenesis. (**A**) Confocal images of a syncytium at day 3. The cell was fixed and stained for actin (red), the plasma membrane (green) and the nucleus (blue). Scale bars: 50 μm. Left: an image of the bottom (underside) of the cell. Center: an image of the middle of the cell. Right: z-sectioning of the cell. (**B**) Images of a cell that was fixed and stained for actin and tubulin. Scale bar: 20 μm. (**C**) A live-cell image of a RAW264.7 cell that was transfected with EGFP–actin (day 3). Scale bar: 20 μm. Inset: a magnified image of the zipper-like structure. Scale bar: 5 μm. (**D**) Live-cell images of four types of actin superstructure found in osteoclasts. We classified osteoclasts into four types; with podosome clusters, with podosome rings, with a cluster of zipper-like structures and with a podosome belt. Arrows indicate each actin superstructure in osteoclasts. Scale bars: 50 μm. (**E**) RANKL-primed mononuclear bone marrow macrophages from ddY, C57BL and ICR mice were seeded on a dentine slice and induced to differentiate into osteoclasts. F-actin was detected by Rhodamine–phalloidin staining. Osteoclasts formed a cluster of actin rings. Arrows indicate the zipper-like structure at the contact site of actin rings. Scale bars: 10 μm.

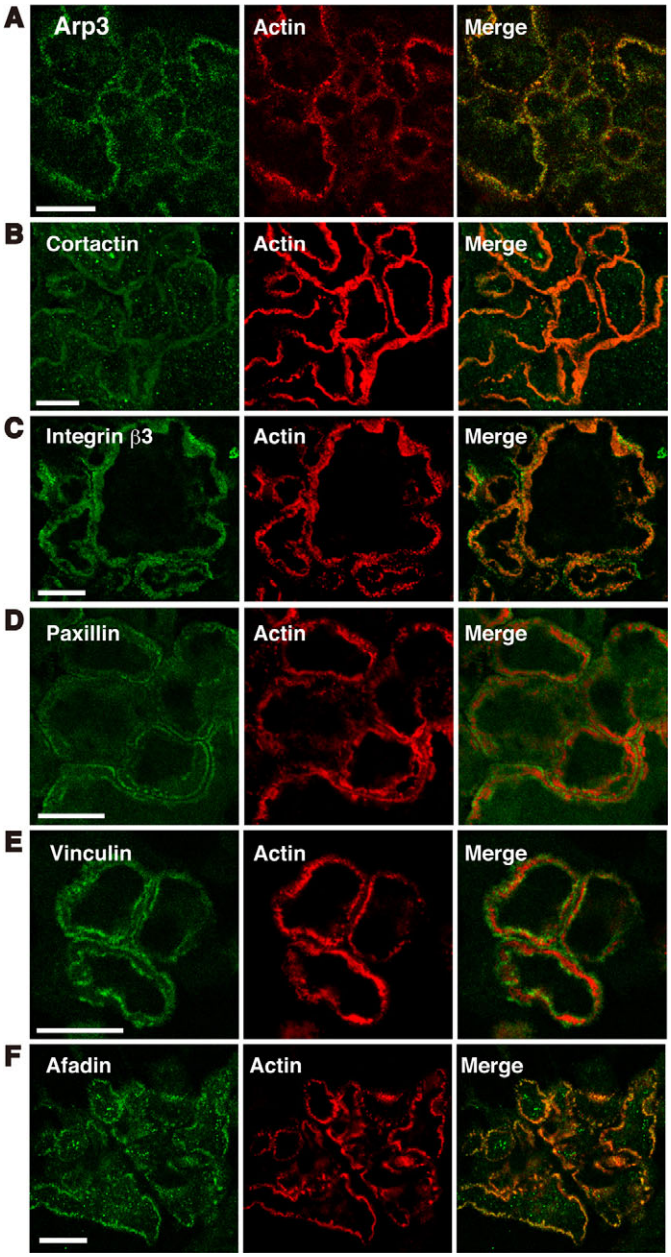

Fig. 3. Colocalization of actin and podosome-related proteins in the zipper-like structure. Confocal images of a syncytium. RAW 264.7 cells were induced to differentiate into osteoclasts by RANKL. At day 3, the cell was fixed and stained for actin (red) and Arp3 (**A**), cortactin (**B**), integrin β3 (**C**), paxillin (**D**), vinculin (**E**) or afadin (**F**; all green). Scale bars: 20 μm.

Compartmentalization of the ventral membrane by the F-actin superstructures

Next, we investigated the relationship between the compartmentalization of the ventral plasma membrane and the zipper-like structure in syncytia. In some instances, a WGA-lectin-positive line was observed in the center of the zipper-like structure (Fig. 4A). Another general plasma-membrane-labeling reagent PKH26 also produced a compartmentalized staining pattern in the ventral membrane (Fig. 4B). A differential interference contrast image of a live cell showed that a phase difference existed at the center of the zipper-like structure (Fig. 4C). These results suggest that the ventral plasma membrane of syncytia is still divided into distinct domains and the zipper-like structures are present at the boundary of the domains.

To further elucidate the nature of the compartmentalization of the ventral membrane by the zipper-like structures, we used a cell-surface biotinylation technique. Live RAW 264.7 cells were labeled with a sulfo-N-hydroxysuccinimide (NHS) biotinylation reagent that recognized primary amines of proteins on the cell membrane, then fixed, permeabilized and stained with Rhodamine–phalloidin and fluorescein–streptavidin. Like the WGA–lectin-staining pattern (Fig. 4A), biotin labeling showed the compartmentalization of the ventral membrane of the syncytia at 3 days after RANKL stimulation (Fig. 4D, upper panel). Biotin labeling encircled a rosette-like structure in mononuclear cells (Fig. 4D, center panel). Interestingly, podosomes at the ventral membrane of RAW 264.7 cells were negative for biotinylation (Fig. 4D, lower panel). The results suggest that the podosome and the podosome-derived actin superstructures form local areas that are inaccessible to biotin in the ventral membrane of RAW 264.7 cells.

These observations raise the next question of whether the zipper-like structures might function as diffusion barriers in the ventral membrane of the syncytia. This was examined in mononuclear RAW 264.7 cells that were cultured for 2 days in the presence of RANKL and labeled with PKH26 (red) or PKH67 (green). The labeled cells were mixed and again induced to differentiate with RANKL. In this assay, a cell resulting from the fusion of a PKH26-labeled cell and a PKH67-labeled cell appeared yellow (Fig. 4E, upper panel). Confocal microscopy of the ventral membranes of the syncytia showed that most compartments enclosed by the zipper-like structures were doubly labeled with green and red dots (Fig. 4D, lower panel). Thus, it is reasonable to conclude that each compartmentalized domain has mixed membrane components derived from mononuclear precursors. Again, the zipper-like structure was free of the labels.

Fine structure of the zipper-like structure

We next examined the fine structure of the zipper-like structure of osteoclasts by transmission electron microscopy. It has already been reported that the actin-based rosette-like structure is free from any prominent intracellular organelles in Rous sarcoma virus-transformed BHK21 cells (Ochoa et al., 2000). When a syncytium with a cluster of actin rings was cut parallel to the substratum, the actin ring was full of randomly oriented F-actin. We could not detect a typical bundle of actin filaments. There were some electron-dense spots and stripes composed of loosely bundled actin filaments near the contact site of actin rings (Fig. 5A). The intensity of these spots and stripes equaled that of the actin core of the podosome (Fig. 5B). The actin ring extended many processes to the outside. The contact site of the actin ring showed an electron-dense membrane-like structure. These results suggest that electron-dense areas at the contact site of actin rings correspond to the zipper-like structures observed by confocal microscopy.

Dynamics of the zipper-like structure

To monitor the dynamics of the zipper-like structure in syncytia, we obtained time-lapse recordings of RAW 264.7 cells that had been transfected with EGFP–actin. Time-lapse

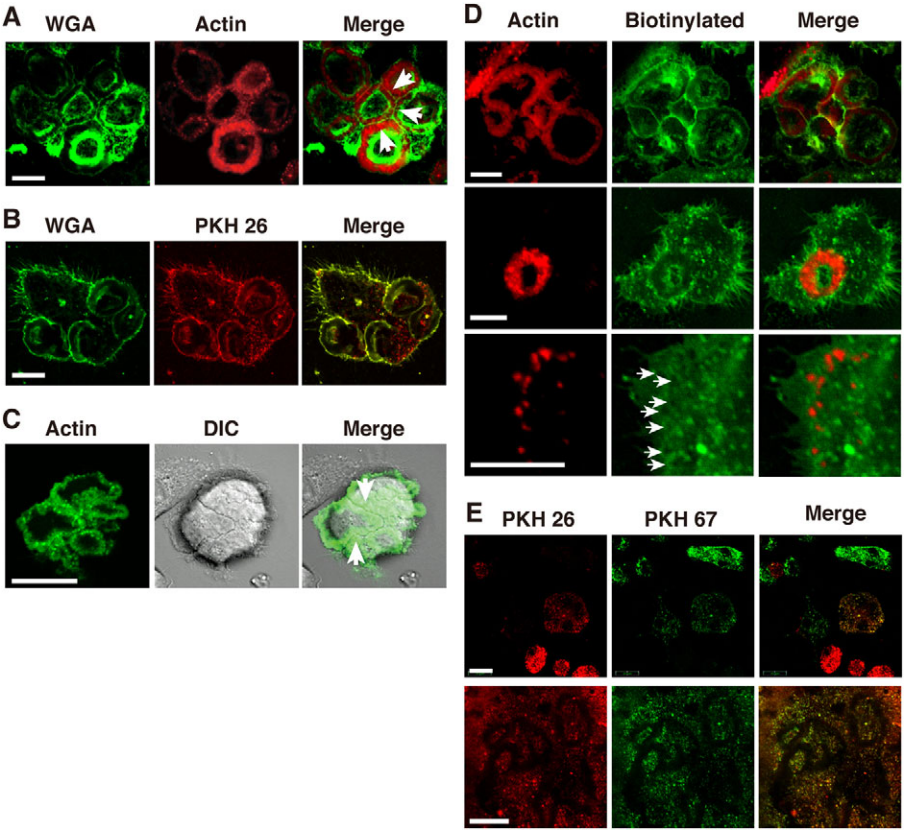

Fig. 4. Compartmentalization of the ventral membrane by a cluster of zipper-like structures. (**A**) A syncytium that was stained with WGA–lectin (green) and for actin (red). Arrows indicate a WGA–lectin-positive line. (**B**) A syncytium that was stained with WGA–lectin (green) and PKH26 (red). (**C**) A differential interference contrast (DIC) image of the bottom of a live syncytium transfected with EGFP–actin. Arrows indicate a line of phase difference. (**D**) Cell surface biotinylation experiments. RAW264.7 cells were biotinylated, fixed and stained for actin (red) and with streptavidin (green). Upper panel: a cluster of zipper-like structure in a syncytium. Middle panel: a rosette in a mononuclear cell. Lower panel: podosomes at the cell periphery of an osteoclast. Arrows indicate the absence of biotin labeling in the podosomes. (**E**) RANKL-primed mononuclear RAW 264.7 cells were tagged with PKH26 (red) or PKH67 (green). They were mixed and induced to differentiate into osteoclasts by RANKL. Upper panel: the tagged cells. Singly tagged cells look red or green. A fused cell with precursors tagged with different colors looks yellow. Lower panel: the bottom of a syncytium. Thick black lines indicated the zipper-like structures. The compartments encircled by the zipper-like structures contained both the red and green dots. Scale bars: 20 μm (A,B,C,E) and 10 μm (D).

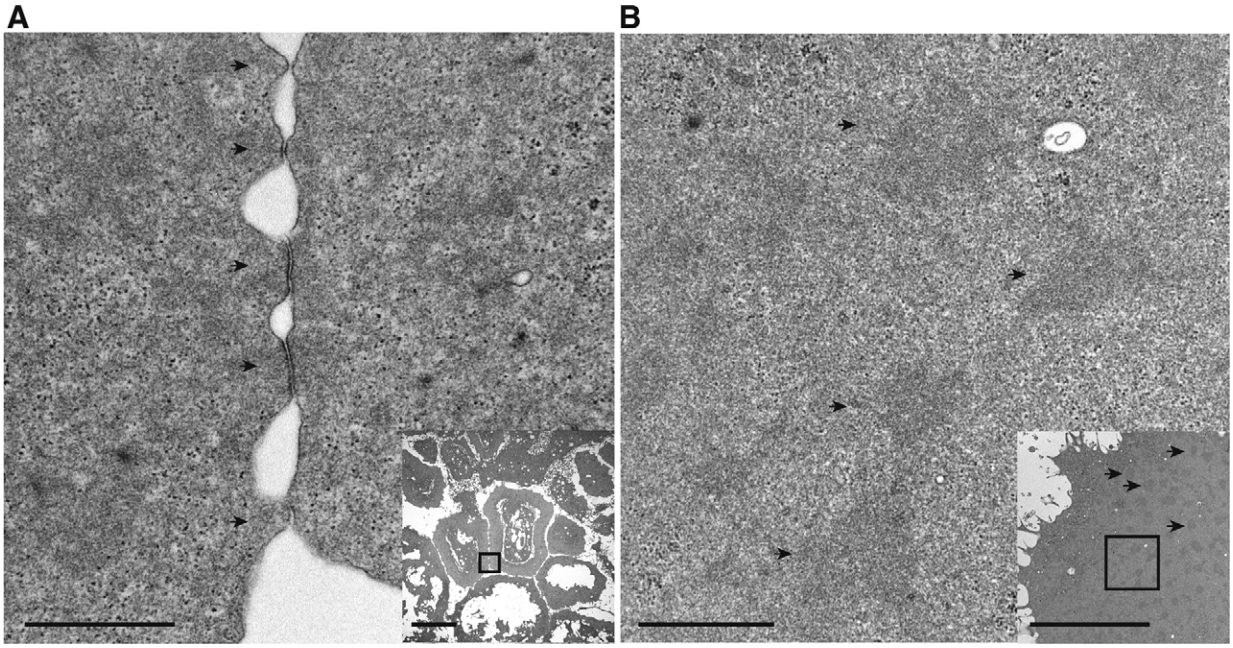

Fig. 5. Ultrastructure of the zipper-like structure. RAW 264.7 cells were cultured with RANKL for 3 days and then fixed and processed for transmission electron microscopy. (**A**) A contact site of the actin rings. The actin ring contains randomly oriented actin filaments and a small number of loose bundles of actin filaments. Processes of the rings touch each other (arrows). The process has an electron-dense membrane-like border. Inset: low-powered view of the cluster of actin rings. A box indicates the magnified area. (**B**) Podosomes. The actin core of the podosome is organized with loose bundles of actin filaments (arrows). Inset: low-powered view of podosomes. Dark areas (arrows) indicate the actin core of the podosomes. A box indicates the magnified area. Scale bars: 1 μm (magnified images) and 10 μm (insets).

recording of the zipper-like structure indicated that the fine morphology of the zipper-like structure was reorganized within 1 minute (Fig. 6A). This rapid turnover rate is similar to those of podosomes and podosome rings (Destaing et al., 2003). Although the individual zipper-like structures were rapidly turned over, the syncytia retained their compartmentalized layout for several hours in the stationary phase (supplementary material Movie 1). The number of compartments delimited by the zipper-like structure was decreased by the destruction of the zipper-like structure from one of its ends (Fig. 6B). Over time, the cluster of zipper-like structures formed a large podosome belt seen in osteoclasts (Fig. 6C). Therefore, the zipper-like structure has the ability to self-assemble, similar to podosomes (Destaing et al., 2003).

Bigger syncytia form the zipper-like structure during the primary fusion

To assess the role of the zipper-like structure in the multinucleation of osteoclasts, we counted the number of nuclei in syncytia with podosome clusters and those with zipper-like structure clusters (Fig. 7A). The histogram for the syncytia with zipper-like structure clusters did not fit a Gaussian distribution (Fig. 7B). Secondary and higher-order cell fusion processes (fusion between a mononuclear cell and a multinucleated cell or between multinucleated cells) probably contributed to the right tail of the histogram. Owing to the deviation from a Gaussian distribution, we prefer to use the median and mode values rather than the average. Seventy-five percent of syncytia with podosome clusters contained fewer than 10 nuclei, whereas 77% of those with zipper-like structure clusters contained more than 10 nuclei. Statistical analysis of these data showed that the former had the median and mode values of 6 and 4, respectively (supplementary material Table S1). By contrast, the values for the latter group were 18 and 13, respectively. Thus, the syncytia with zipper-like structure clusters had more nuclei than those with podosome clusters ($P<0.001$). The zipper-like structure appears to be a device for more efficient multinucleation than the podosome clusters. A similar analysis was performed on differentiated osteoclasts from RAW 264.7 cells (Fig. 7C). To understand the role played by actin superstructures in multinucleation, we classified osteoclasts into four types: osteoclasts with podosome clusters, those with podosome rings, those with a cluster of zipper-like structures and those with a podosome belt (Fig. 2D). As a result, we found that 43% and 47% of osteoclasts possessed podosome clusters and a podosome belt, respectively (Fig. 7D). We then used these values to construct a theoretical histogram for differentiated osteoclasts from the values observed for syncytia on day 3 (Fig. 7C). The difference between the theoretical and observed distributions was statistically insignificant ($P<0.574$). This strengthens the notion that the syncytia with zipper-like structure clusters on day 3 become osteoclasts with podosome belts on day 4, which is in agreement with our time-lapse observations (Fig. 6C).

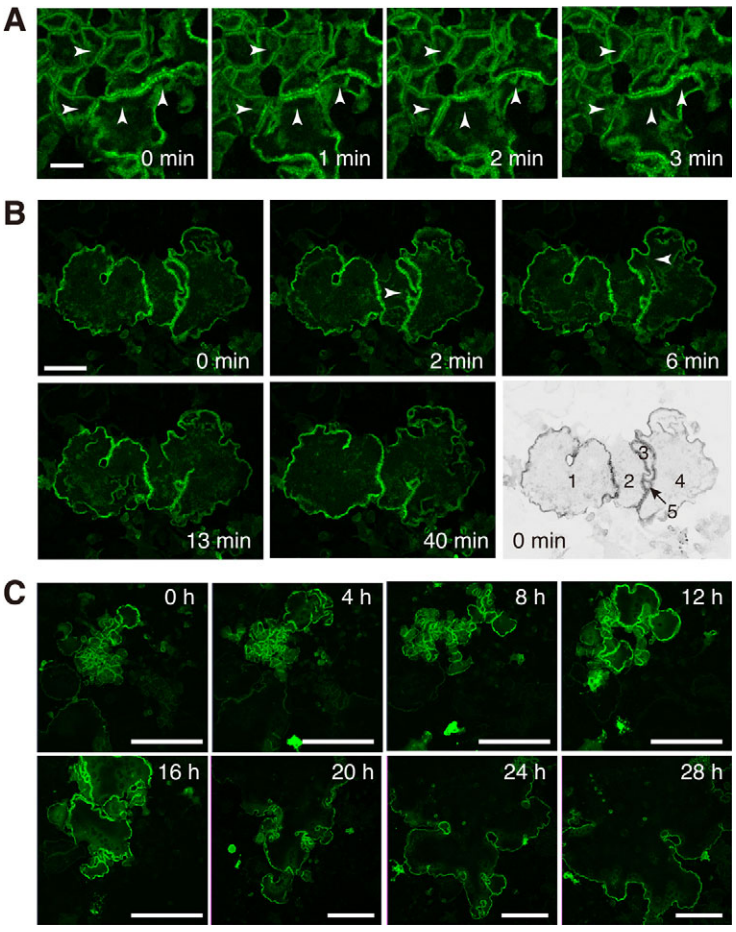

Fig. 6. Dynamics of the zipper-like structure. (**A**) Time-lapse images of a syncytium that was transfected with EGFP–actin, taken on day 3. The arrowheads indicate the reorganization of the zipper-like structures. Scale bar: 20 μm. (**B**) Decrease in the number of compartments due to the breakdown of the zipper-like structures. At time 0 minutes, the ventral membrane of the syncytium is divided into five compartments by the zipper-like structures. The zipper-like structures between compartments 2 and 3, and 3 and 4, began to disappear at 2 and 6 minutes, respectively. Compartments 2, 3 and 4 have become one compartment by 40 minutes. Arrowheads indicated that the destruction of the zipper-like structure proceeded from one of its edges. Scale bar: 50 μm. (**C**) Evolution of the zipper-like structure. Repeated breakdown of the zipper-like structures results in the formation of a podosome belt by 12 hours. Subsequently, the podosome belt fuses with neighboring belts and expands in size. The digital magnification was reduced to 67% between 16 hours and 20 hours. Scale bars: 200 μm.

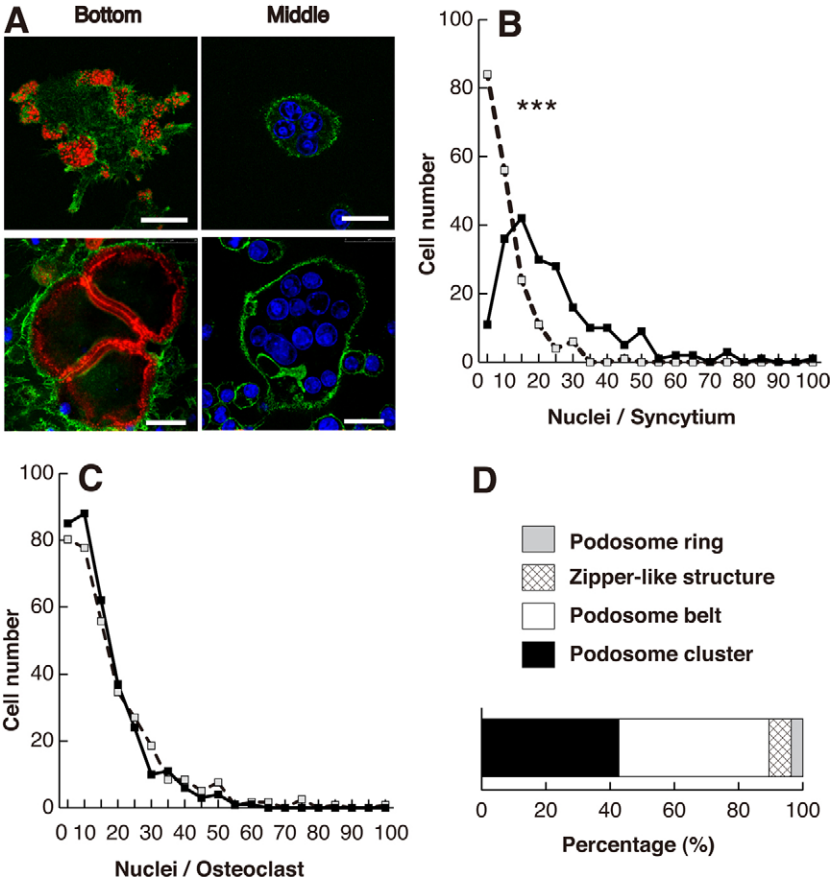

Fig. 7. Efficient multinucleation of a syncytium containing a cluster of the zipper-like structures. (**A**) Representative images of a syncytium with podosome clusters (upper panel) and another with a cluster of zipper-like structures (lower panel). On day 3 of culture, the cells were fixed and stained for F-actin (red), the plasma membrane (green) and the nucleus (blue). Scale bars: 20 μm. (**B**) Histograms of the number of the nuclei per syncytium on day 3. The number of nuclei in syncytia with more than three podosome clusters (broken line) or three zipper-like structures (solid line) was counted; $n=186$ for podosome clusters, $n=207$ for zipper-like structures. Data are the sum of six separate experiments. ***$P<0.001$. (**C**) Histograms of the number of the nuclei per osteoclast. The solid line indicates the numbers of osteoclasts with more than three nuclei on day 4; $n=332$. Data are the sum of four separate experiments. The broken line is a theoretical curve calculated from the data for syncytia with podosome clusters and those with zipper-like structures shown in B. The percentages of each type were taken from Fig. 7D. Total cell number was corrected to 332, the actual cell number. (**D**) Percentage of osteoclasts with different actin superstructures. The osteoclasts in C were classified into the four types.

Matured osteoclasts form the zipper-like structure during the secondary fusion

We also observed similar zipper-like structures in mature osteoclasts derived from RAW264.7 cells, on day 4 (Fig. 8A,B). The osteoclasts with the zipper-like structure contained more nuclei than the average sized osteoclasts. The median and mode values of the former were 23 and 17, and the values for the latter were 10 and 3, respectively (supplementary material Table S1). Time-lapse confocal microscopy of RAW264.7 cells transfected with EGFP–actin enabled us to monitor the fusion between multinucleated osteoclasts (Fig. 8C). The two osteoclasts stayed attached for some time before fusion (60±7.2 minutes; $n=6$). The two osteoclasts probably formed the zipper-like structure at the contact site during this time. The podosome belts at the contact site broke down following membrane fusion, resulting in the fusion of podosome belts of distinct osteoclasts. The process of breakdown of the podosome belt at the contact site was quite similar to that of the zipper-like structure observed in the syncytium (Fig. 6B). The results show that terminally differentiated osteoclasts have the ability to fuse again, forming secondary and higher-order fusions. It further suggests the possible role of the zipper-like structure in osteoclasts as cell–cell adhesion machinery.

The zipper-like structure in the sealing zone of osteoclasts in vivo

We previously developed an in vivo assay system for the F-actin structure in the clear zone of osteoclasts, using rat calvariae (Kuroda et al., 1996; Nakamura et al., 1996). The same method was applied to postnatal day 0 (P0) to P14 ddY mouse calvariae. A ring-shaped F-actin structure appeared on P1 at the endocranial surfaces of parietal bones near to the sutura sagittalis. The number of the F-actin rings increased until P8 and decreased thereafter. Most cells with the F-actin rings contained cathepsin K, a marker of osteoclasts, inside of the ring (Fig. 9A). The cells with the actin rings had many nuclei (Fig. 9B). Thus, the actin ring probably represents the F-actin structure in the sealing zone of the actively resorbing osteoclast. Most F-actin rings were single and independent. However, some rings formed a cluster between P7 and P10 (Fig. 9C). We often observed the zipper-like structure at the interface of two such actin rings (Fig. 9D). There was a WGA–lectin-positive line along the center of the zipper-like structure, similar to those observed in the syncytium (Fig. 4A) and the multinucleated cells (Fig. 8B) derived from RAW264.7 cells. The results suggest that osteoclasts in mouse calvariae also form the actin-based zipper-like structure in the sealing zone.

Discussion

Our study adds a zipper-like structure to the repertoire of actin-based osteoclast superstructures. Because the zipper-like structure is found in the ventral membrane of syncytia and matured osteoclasts, it is thought to play a role in cell–matrix adhesion. Indeed, the zipper-like structure contains integrin β3 and the integrin-associated proteins paxillin and vinculin, similar to the podosome (Fig. 3). This further supports the zipper-like structure having a cell–matrix adhesion function. However, several pieces of evidence suggest that it might have other

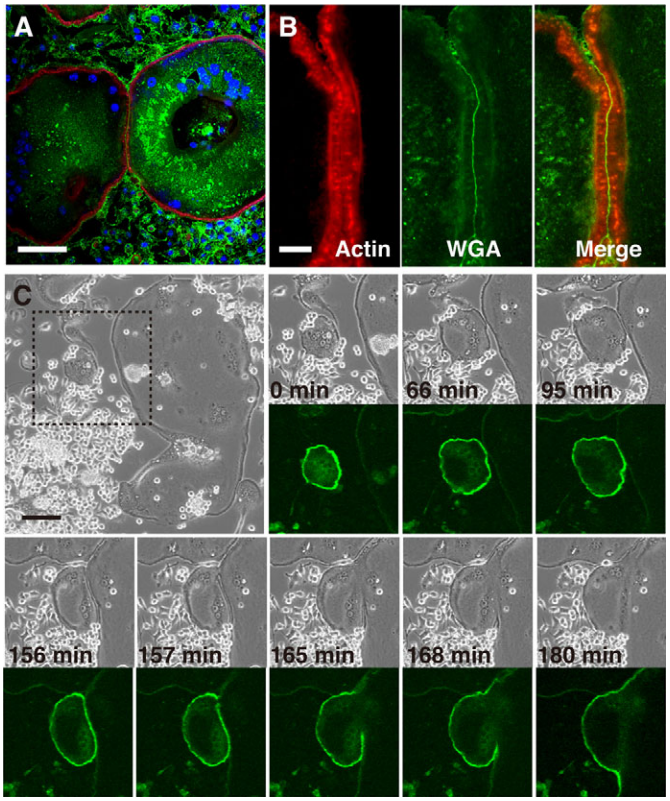

Fig. 8. The zipper-like structure at the cell contact site of osteoclasts. (**A**) A confocal image of two osteoclasts derived from RAW264.7 cells, at day 4, stained for actin (red), the plasma membrane (green) and the nucleus (blue). Scale bar: 50 µm. (**B**) An enlarged image of the cell–cell contact site in A. Scale bar: 10 µm. (**C**) Time-lapse confocal recording performed with RAW264.7 cells transfected with EGFP–actin. The experiment was performed on day 4 after the addition of RANKL. Images were captured every minute. At time 0 minutes, an osteoclast on the left had 7 nuclei and an osteoclast on the right had 56 nuclei. Two separate cells came in contact at 66 minutes and formed a zipper-like structure at 95 minutes. There was a lag until 156 minutes. The cell fusion started at 157 minutes. The EGFP-negative gap widened until 168 minutes. Reshaping of the fused belt then followed. A dashed box in the first image indicates the area used for time-lapse observation. Upper panels, phase contrast; lower panels, EGFP–actin. Scale bar: 100 µm.

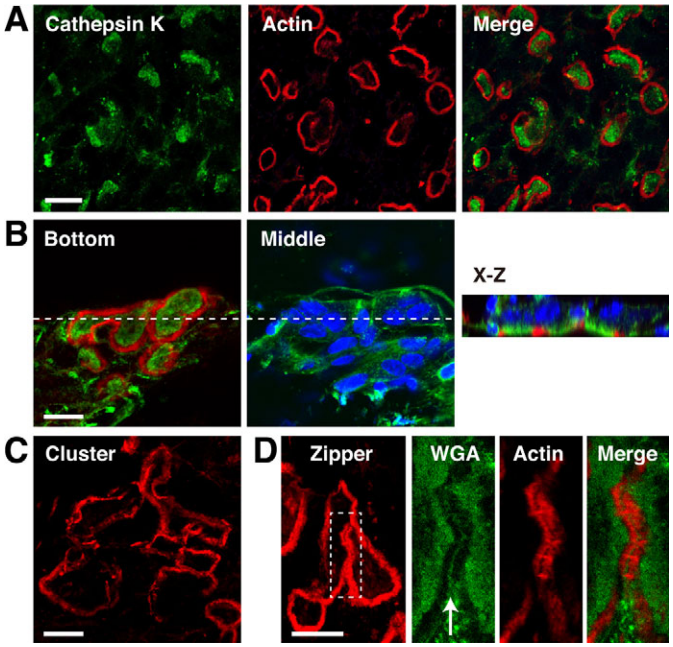

Fig. 9. The zipper-like structure in the sealing zone of osteoclasts. (**A**) A calvaria from a P9 ddY mouse stained for cathepsin K (green) and F-actin (red). (**B**) A calvaria from a P5 ddY mous stained for WGA–lectin (green), the nucleus (blue) and F-actin (red). Left: an image of the bottom of the cells. Center: an image of the middle of the cells. Right: a z-section of cells sliced at the white line shown in the left panels. (**C**) A cluster of the zipper-like structures in a P7 calvaria. (**D**) Two actin rings formed a zipper-like structure at the contact site in a P8 calvaria. A white box indicates the area enlarged in the right panels. A WGA–lectin-positive line runs along the center of the zipper-like structure (arrow). Most images presented are projections of 5−25 µm. Scale bars: 20 µm.

functions. First, it resembles the morphology of the adhesion zipper found in keratinocytes. The function of the adhesion zipper is to link the neighboring cells to form an epithelial sheet. This coincides with the formation of the zipper-like structure at the cell contact site of matured osteoclasts before cell fusion (Fig. 8). Second, it contains the cell–cell adhesion molecule afadin. Third, the syncytia containing a cluster of the zipper-like structures have more nuclei than those without them. These lines of evidence support the view that the zipper-like structure is involved in adhesion of neighboring cells. However, the syncytia with the zipper-like structure has already completed membrane fusion dorsally (Fig. 2A), which suggests that the zipper-like structure is not involved in cell–cell adhesion. Future experiments are needed to reconcile this inconsistency.

The zipper-like structure has distinct structural characteristics. First, the arrangement of its components is similar to that in the podosome and podosome belt: the actin core region contains Arp3 and cortactin, whereas the surrounding region consists of integrin and integrin adhesion-associated proteins (Fig. 3). Second, the zipper-like structure does not show any WGA–lectin staining, or biotin, PKH26 or PKH67 labeling (Fig. 4A,D,E) and seems to compartmentalize the ventral membrane. This property indicates that the zipper-like structure has a barrier function against the lateral diffusion of membrane proteins. However, the mixing experiments with PKH26- and PKH67-tagged cells showed that it did not have this function. Because the PKH labeling in RAW 264.7 cells were distributed not only in the plasma membrane but also in the endosome-like vesicles in the cytoplasm, there is a possibility that the mixing of labeling reagents in the compartment was mainly due to the vigorous exocytic transport of labels to the compartments, but not the lateral diffusion across the zipper-like structures in the ventral membrane. Future experiments using quantitative live-cell imaging are needed to exclude this possibility. Third, the superstructure transiently appears in the course of differentiation after the aggregation of mononuclear precursor cells and before terminal differentiation, represented by the podosome belt formation (Fig. 1C, Fig. 6C). A similar zipper-like structure is also observed when two matured osteoclasts stay attached before membrane fusion (Fig. 8). The time frame of the appearance of the zipper-like structure probably rules out a direct role of the superstructure in the membrane fusion. Lastly, the fine structure of the zipper-like structure is reorganized within 1 minute (Fig. 6A and supplementary material Movie 1). This

could be due to the vigorous assembly and disassembly of local actin filaments such as those in podosomes (Destaing et al., 2003). The actin filaments at the cell contact sites of Madin–Darby canine kidney (MDCK) cells fluctuate with a half-life ~0.2 minutes (Yamada et al., 2005). We obtained a comparable value for the half-life of the zipper-like structure in osteoclasts by fluorescence recovery after photobleaching (FRAP) measurements (data not shown). This dynamic character might be the reason that no bundled filaments were apparent in the zipper-like structure using electronmicroscopy (Fig. 5). By contrast, bundled actin filaments in the adhesion zipper in keratinocytes are clearly visible (Vasioukhin et al., 2000). Therefore, it would be interesting to examine the dynamics of actin bundles in the adhesion zipper by FRAP analysis.

The finding of the zipper-like structure in syncytia has revealed an alternative pathway for osteoclast multinucleation (Fig. 10). The existing model states that mononuclear precursors with multiple podosomes collide and fuse to form an osteoclast. Podosomes develop into podosome clusters, podosome rings, and finally a podosome belt (Jurdic et al., 2006). In the alternative pathway, mononuclear precursors use the zipper-like structure to make larger aggregates, resulting in larger osteoclasts, and the cluster of zipper-like structures develops into a podosome belt in the differentiated osteoclast. This scenario allows precursors to 'choose' whether to become a small or big osteoclast. This decision-making process must be context-dependent, and the alternative pathways are considered to be independent. Because the zipper-like structure was found in the mouse calvariae (Fig. 9), this two-route model could provide insights into the in vivo generation of hypermultinucleated osteoclasts in physiological and pathological conditions. In fact, some isolated multinucleated cells obtained from giant cell tumors of bone exhibit characteristics similar to those of hypermultinucleated osteoclasts, i.e. compartmentalization and the zipper-like structure discussed above (Kanehisa et al., 1991).

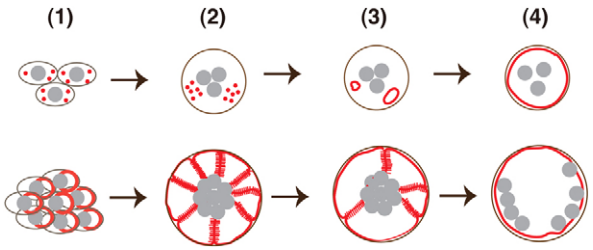

Fig. 10. Two models of osteoclast multinucleation. Upper image: multinucleation without the zipper-like structure. Mononuclear cells with podosomes clusters collide (1) and fuse to form a small osteoclast with podosome clusters (2). The podosome clusters develop into podosome rings (3) and subsequently, a podosome belt (4) after cell fusion. Adopted and modified from Destaing et al. (Destaing et al., 2003). Lower image: multinucleation involving the zipper-like structure. Mononuclear cells with actin rings collide (1), forming a cluster of zipper-like structures in syncytia (2). Breakdown of the zipper-like structures (3) leads to the formation of a podosome belt in the differentiated osteoclast (4). This type of multinucleation produces a larger osteoclast. 1. Collision of fusion competent mononuclear cells. 2. A syncytium after membrane fusion. 3. Rearrangement of the actin superstructure. 4. The product of primary fusion (fusion of mononuclear cells), which has a podosome belt. The red line represents actin-based superstructures in the ventral membrane. The gray circles represent the nuclei.

In conclusion, osteoclasts employ distinct actin superstructures depending on their sizes during the cell fusion stage. Elucidation of the structure and function of the zipper-like structure might lead to selective therapeutics for the bone diseases caused by hypermultinucleated osteoclasts.

Materials and Methods

Materials

The reagents used were obtained from the following sources: α-minimum essential medium (α-MEM; WAKO, Osaka, Japan); fetal bovine serum (FBS; Sigma); anti-Arp3 (Santa Cruz); anti-integrin β3 (clone 2C9.G2; Biolegend, San Diego, CA); anti-AF-6/Afadin (Santa Cruz); anti-β-catenin (BD Biosciences); anti-cathepsin K (Daiichi Fine Chemical Co., Toyama, Japan); anti-cortactin (Upstate Millipore); anti-E-cadherin (N-20, Santa Cruz; ECCD-1, TaKaRa, Shiga, Japan); FITC–WGA–lectin (Sigma); anti-pan-cadherin (Sigma); anti-paxillin (BD Biosciences); anti-vinculin (Sigma); Rhodamine–phalloidin and TOTO-3 (Molecular Probes); recombinant human macrophage colony-stimulating factor (hM-CSF, leukoprol; Kyowahakko, Tokyo, Japan); and recombinant mouse soluble (s) RANKL (PeproTech, Rocky Hill, NJ); EZ-Link Sulfo-NHS-LC-biotin (Thermo Scientific Pierce); PKH26 and PKH67 (Sigma); dentine slices and collagenase (WAKO).

Detection of F-actin in the clear zone

Distribution of F-actin in the mouse calvariae was detected as previously described with slight modifications (Kuroda et al., 1996; Nakamura et al., 1996). All procedures were performed at room temperature. Calvariae were dissected from ddY mice and fixed with 4% paraformaldehyde in PBS (pH 7.4) for 30 minutes. After a thorough rinse in PBS, specimens were cut and trimmed in small pieces, treated with 0.05% collagenase in PBS for 10 minutes, followed by incubation with 0.5% NP-40 in PBS for 10 minutes. Then, periosteal membranes were carefully scraped from the endocranial and outer surfaces of the calvariae under a dissecting microscope. The specimens were blocked with 1% BSA in PBS for 1 hour, incubated with the anti-cathepsin K antibody for 1 hour, then incubated with the secondary antibody, Rhodamine–phalloidin, FITC–WGA–lectin and/or TOTO-3. Confocal images were obtained using Olympus IX71 inverted microscope and Zeiss LSM510 confocal imaging system.

Osteoclastogenesis

RAW 264.7 cells ($1\sim2\times10^4$) were seeded on a glass coverslip (Fisher Scientific, Thermo Scientific, IL), placed in a 24-well culture dish in 0.5 ml α-MEM, 10% FBS, antibiotics, 0.1 mM non-essential amino acids and 100 ng/ml sRANKL, and cultured to induce osteoclastogenesis. Under these conditions, RAW 264.7 cells form syncytia by day 3 and mature osteoclasts with podosome belts by day 4.

Osteoclasts were also induced from mouse bone marrow cells as follows. Bone marrow cells were collected from the tibiae of 6- to 8-week-old C57BL, ddY or ICR mice. They were incubated with red blood cell lysis buffer (Roche) for 1 minute and washed three times with Dulbecco's PBS (D-PBS). The obtained bone marrow cells (1×10^7) were cultured overnight in a 10-cm Petri dish with α-MEM, 10% FBS, 0.1 mM non-essential amino acids and 1/50 (vol/vol) of CMG14-12 culture supernatant (CMG) (Takeshita et al., 2000). Next day, the floating cells were transferred to a new 10-cm Petri dish with the fresh medium. After culturing for 3 days, the adherent cells were recovered by trypsinization and further cultured for 2 days in a 5-cm culture dish with α-MEM, 10% FBS, 0.1 mM non-essential amino acids, 100 ng/ml sRANKL and 3×10^3 IU/ml human M-CSF. The RANKL-primed mononuclear cells were removed from the dish by incubating with PBS containing 20 mM glycine for 5 minutes, with mechanical shaking. The recovered cells (1.5×10^5) were seeded on a dentine slice placed in a 48-well culture dish and cultured for 2 days in 0.25 ml of the medium containing sRANKL and M-CSF as described above. The cells on a dentine slice were fixed, permeabilized and stained with Rhodamine–phalloidin for confocal microscopy. Because the surface of a dentine slice was rough, the confocal images shown are projections from 5–7 μm. All animals used were treated in accordance with The Guidelines for the Care and Use of Animals, of Keio University School of Medicine.

Cell surface biotinylation

RAW 264.7 cells cultured on a glass coverslip for 3 days were washed three times with PBS (pH 8.0) containing 0.1 mM $CaCl_2$. The cells were incubated with 5 mM EZ-Link Sulfo-NHS-LC-biotin in PBS (pH 8.0) containing 0.1 mM $CaCl_2$, for 3–10 minutes. Biotinylation was stopped by washing three times with TBS (pH 7.6) containing 0.1 mM $CaCl_2$ followed by fixation with 4% paraformaldehyde for 15 minutes. $CaCl_2$ was added to prevent the detachment of cells from a glass surface. The fixed cells were permeabilized with 0.5% NP-40 in PBS for 10 minutes and blocked with 1% BSA in PBS for 1 hour. The cells were incubated with fluorescein–streptavidin (Vector Laboratories) and Rhodamine–phalloidin in PBS containing 0.1% BSA for 30 minutes for confocal microscopy.

Cell labeling with PKH26 and PKH67

RAW 264.7 cells (8×10^5) were seeded in a 10-cm culture dish and cultured in 10 ml α-MEM, 10% FBS and antibiotics, containing 100 ng/ml RANKL, for 2 days. The adherent mononuclear cells were removed from the dish by incubating with D-PBS containing 20 mM glycine for 5 minutes with mechanical shaking. The recovered cells were labeled with PKH26 (red) or PKH67 (green) according to the protocol provided by the manufacturer (Sigma). Mononuclear cells (2×10^6) were incubated with 4 µl PKH26 or PKH67 in 200 µl of diluent C for 10 minutes. The cells (1.5×10^4) labeled with PKH26 or PKH67 were mixed and seeded on a glass coverslip in a 24-well culture dish. The mixed cells were cultured for 2 days in 0.5 ml α-MEM, 10% FBS, 100 ng/ml RANKL, containing 5 mM NH_4Cl, and fixed with 4% paraformaldehyde for confocal microscopy. Because the labeling reaction itself inhibited the formation of zipper-like structures, we added NH_4Cl to the culture medium to increase the number of the zipper-like structures. The fluorescence of PKH26 and PKH67 was recorded in the Rhodamine and FITC channel, respectively, of the Fluoview FV300 software for the Olympus IX71.

Counting of nuclei in the cells

All cells were cultured on glass coverslips (Fisher Scientific). At 3 or 4 days after the addition of RANKL, the cells were fixed with 4% paraformaldehyde, permeabilized with 0.5% NP-40, and stained for actin (Rhodamine–phalloidin), the plasma membrane (WGA-lectin) and the nucleus (TOTO-3). The stained cells were processed for confocal microscopy and then the underside of the cells were photographed in order to detect actin superstructures, and the middle of the cells was photographed to count the number of nuclei. Cells with more than three nuclei were selected for all counting experiments. On day 3, syncytia with more than three podosome clusters or more than three zipper-like structures were carefully chosen (Fig. 7B). Syncytia containing both podosome clusters and zipper-like structures were eliminated from the counts. Data were collected from six independent experiments. On day 4, all the cells with more than three nuclei were chosen, classified into four types and the nuclei were counted (Fig. 7C). The photographed fields were chosen randomly. Data were collected from four independent experiments. A histogram with an interval of five was constructed to show the distribution of the data. Then, a theoretical histogram was constructed by using the experimental data from the syncytia with podosome clusters and those with zipper-like structures (Fig. 7B). According to the results shown in Fig. 7D, the percentage of each cell type was 43% and 47%, respectively. Total cell number was corrected to 332, the actual cell number in Fig. 7C.

Electron microscopy

RAW 264.7 cells were seeded on a 35 mm glass-bottomed dish with grids (Matsunami, Osaka, Japan) at a density of 1.5×10^4 cells in 0.5 ml α-MEM, 10% FBS, antibiotics and 100 ng/ml RANKL, and cultured for 3 days. The cells were fixed with 2% glutaraldehyde, 2% paraformaldehyde and 0.1 M PBS (pH 7.4) at 37℃ for 15 minutes. The specimen was further fixed with 2% glutaraldehyde and 0.1 M PBS (pH 7.4) at 4℃. The cells were postfixed with OsO_4, dehydrated and embedded in Quetol-812 (Nisshin EM, Tokyo, Japan). The glass was dissolved by incubating with hydrofluoric acid at room temperature for 20 minutes. Sections (70 nm thick) were obtained by cutting parallel to the substratum. Sectioning was performed between 0.5 and 0.6 µm above the substratum. The sections were stained with uranyl acetate and lead citrate. Photographs were taken on JEM-1200EX electron microscope (JOEL, Tokyo, Japan) at 80 kV.

Immunofluorescence and live-cell imaging

For confocal microscopy, the cells were fixed with 4% paraformaldehyde in PBS for 30 minutes, permeabilized with 0.5% NP-40 in PBS for 15 minutes, and blocked with 1% BSA in PBS for 1 hour. The fixed cells were then incubated with the primary antibodies for 1 hour, before being incubated with the secondary antibody (Rhodamine–phalloidin or TOTO-3). Confocal images were obtained using an Olympus IX71 and a Leica TCS-SP5 (Leica, Wetzlar, Germany) confocal microscope.

Time-lapse confocal images were obtained with a Zeiss LSM 780 (Carl Zeiss Microimaging, Tokyo, Japan) and an Olympus FV10i (Olympus) microscopes. RAW264.7 cells were plated on a 35 mm glass-bottomed culture dish (MatTek, MA). The cells were then transfected with EGFP–actin (Clontech, CA) using the FuGENE HD transfection reagent (Roche) according to the protocol provided, and allowed to differentiate into osteoclasts. The culture medium was supplemented with 100 ng/ml RANKL just before each recording. Long-term (over 24 hours) and differential interference contrast recording were performed using a Zeiss LSM780 in a 5% CO_2 humidified atmosphere at 37℃. The retrieved images were processed with Photoshop CS (Adobe, CA).

Statistical analysis

Microsoft Excel (Microsoft) was used to construct and analyze the histograms. The *P*-values shown in Fig. 7B,C were calculated using the Mann–Whitney two-tailed test, in Prism 5 (GraphPad Software).

Acknowledgements

We thank Y. Nonomura, T. Suda and N. Takahashi for their encouragement; S. Takeshita for a CMG14-12 cell line; N. Shimizu and K. Dan at the Core Instrumentation Facility at Keio University School of Medicine for performing the confocal microscopy; and T. Tanaka and M. Yamaguchi for performing the time-lapse imaging.

Funding

This work was supported in part by Grants-in Aid for Challenging Exploratory Research [grant number 19659387 to J.T.]; and The Fugaku Trust For Medicinal Research [to J.T].

Supplementary material available online at
http://jcs.biologists.org/lookup/suppl/doi:10.1242/jcs.090886/-/DC1

References

Adams, C. L., Chen, Y. T., Smith, S. J. and Nelson, W. J. (1998). Mechanisms of epithelial cell-cell adhesion and cell compaction revealed by high-resolution tracking of E-cadherin-green fluorescent protein. *J. Cell Biol.* **142**, 1105-1119.

Bozec, A., Bakiri, L., Hoebertz, A., Eferl, R., Schilling, A. F., Komnenovic, V., Scheuch, H., Priemel, M., Stewart, C. L., Amling, M. et al. (2008). Osteoclast size is controlled by Fra-2 through LIF/LIF-receptor signalling and hypoxia. *Nature* **454**, 221-225.

Cavey, M. and Lecuit, T. (2009). Molecular bases of cell-cell junctions stability and dynamics. *Cold Spring Harb. Perspect. Biol.* **1**, a002998.

Destaing, O., Saltel, F., Geminard, J. C., Jurdic, P. and Bard, F. (2003). Podosomes display actin turnover and dynamic self-organization in osteoclasts expressing actin-green fluorescent protein. *Mol. Biol. Cell* **14**, 407-416.

Gardner, C. R. (2007). Morphological analysis of osteoclastogenesis induced by RANKL in mouse bone marrow cell cultures. *Cell Biol. Int.* **31**, 672-682.

Gloushankova, N. A., Krendel, M. F., Alieva, N. O., Bonder, E. M., Feder, H. H., Vasiliev, J. M. and Gelfand, I. M. (1998). Dynamics of contacts between lamellae of fibroblasts: Essential role of the actin cytoskeleton. *Proc. Natl. Acad. Sci. USA* **95**, 4362-4367.

Hall, A. (1998). Rho GTPases and the actin cytoskeleton. *Science* **279**, 509-514.

Helming, L. and Gordon, S. (2009). Molecular mediators of macrophage fusion. *Trends Cell Biol.* **19**, 514-522.

Illes, T. and Fischer, J. (1989). Distribution of lectin binding glycoprotein in osteoclasts. *Histochemistry* **91**, 55-59.

Jurdic, P., Saltel, F., Chabadel, A. and Destaing, O. (2006). Podosome and sealing zone: Specificity of the osteoclast model. *Eur. J. Cell Biol.* **85**, 195-202.

Kanehisa, J., Yamanaka, T., Doi, S., Turksen, K., Heersche, J. N., Aubin, J. E. and Takeuchi, H. (1990). A band of F-actin containing podosomes is involved in bone resorption by osteoclasts. *Bone* **11**, 287-293.

Kanehisa, J., Izumo, T., Takeuchi, M., Yamanaka, T., Fujii, T. and Takeuchi, H. (1991). In vitro bone resorption by isolated multinucleated giant cells from giant cell tumour of bone: Light and electron microscopic study. *Virchows Arch. A Pathol. Anat. Histopathol.* **419**, 327-338.

Kremerskothen, J., Stolting, M., Wiesner, C., Korb-Pap, A., van Vliet, V., Linder, S., Huber, T. B., Rottiers, P., Reuzeau, E., Genot, E. et al. (2011). Zona occludens proteins modulate podosome formation and function. *FASEB J.* **25**, 505-514.

Kurihara, N., Reddy, S. V., Menaa, C., Anderson, D. and Roodman, G. D. (2000). Osteoclasts expressing the measles virus nucleocapsid gene display a pagetic phenotype. *J. Clin. Invest.* **105**, 607-614.

Kurihara, N., Hiruma, Y., Yamana, K., Michou, L., Rousseau, C., Morissette, J., Galson, D. L., Teramachi, J., Zhou, H., Dempster, D. W. et al. (2011). Contributions of the measles virus nucleocapsid gene and the SQSTM1/p62(P392L) mutation to Paget's disease. *Cell Metab.* **13**, 23-34.

Kuroda, H., Nakamura, M. and Kamiyama, K. (1996). Effects of calcitonin and parathyroid hormone on the distribution of F-actin in the clear zone of osteoclasts in vivo. *Bone* **19**, 115-120.

Larsen, M., Artym, V. V., Green, J. A. and Yamada, K. M. (2006). The matrix reorganized: Extracellular matrix remodeling and integrin signaling. *Curr. Opin. Cell Biol.* **18**, 463-471.

Linder, S. (2007). The matrix corroded: Podosomes and invadopodia in extracellular matrix degradation. *Trends Cell Biol.* **17**, 107-117.

Mbalaviele, G., Chen, H., Boyce, B. F., Mundy, G. R. and Yoneda, T. (1995). The role of cadherin in the generation of multinucleated osteoclasts from mononuclear precursors in murine marrow. *J. Clin. Invest.* **95**, 2757-2765.

Nagata, Y. and Burger, M. M. (1974). Wheat germ agglutinin. Molecular characteristics and specificity for sugar binding. *J. Biol. Chem.* **249**, 3116-3122.

Nakamura, M., Kuroda, H., Narita, K. and Endo, Y. (1996). Parathyroid hormone induces a rapid increase in the number of active osteoclasts by releasing histamine from mast cells. *Life Sci.* **58**, 1861-1868.

Ochoa, G. C., Slepnev, V. I., Neff, L., Ringstad, N., Takei, K., Daniell, L., Kim, W., Cao, H., McNiven, M., Baron, R. et al. (2000). A functional link between dynamin and the actin cytoskeleton at podosomes. *J. Cell Biol.* **150**, 377-389.

Roodman, G. D. and Windle, J. J. (2005). Paget disease of bone. *J. Clin. Invest.* **115**, 200-208.

Salo, J., Metsikko, K., Palokangas, H., Lehenkari, P. and Vaananen, H. K. (1996). Bone-resorbing osteoclasts reveal a dynamic division of basal plasma membrane into two different domains. *J. Cell Sci.* **109**, 301-307.

Spinardi, L. and Marchisio, P. C. (2006). Podosomes as smart regulators of cellular adhesion. *Eur. J. Cell Biol.* **85**, 191-194.

Suda, T., Takahashi, N., Udagawa, N., Jimi, E., Gillespie, M. T. and Martin, T. J. (1999). Modulation of osteoclast differentiation and function by the new members of the tumor necrosis factor receptor and ligand families. *Endocr. Rev.* **20**, 345-357.

Takai, Y., Miyoshi, J., Ikeda, W. and Ogita, H. (2008). Nectins and nectin-like molecules: roles in contact inhibition of cell movement and proliferation. *Nat. Rev. Mol. Cell Biol.* **9**, 603-615.

Takeshita, S., Kaji, K. and Kudo, A. (2000). Identification and characterization of the new osteoclast progenitor with macrophage phenotypes being able to differentiate into mature osteoclasts. *J. Bone Miner. Res.* **15**, 1477-1488.

Ueki, Y., Lin, C. Y., Senoo, M., Ebihara, T., Agata, N., Onji, M., Saheki, Y., Kawai, T., Mukherjee, P. M., Reichenberger, E. et al. (2007). Increased myeloid cell responses to M-CSF and RANKL cause bone loss and inflammation in SH3BP2 "cherubism" mice. *Cell* **128**, 71-83.

Vasioukhin, V., Bauer, C., Yin, M. and Fuchs, E. (2000). Directed actin polymerization is the driving force for epithelial cell-cell adhesion. *Cell* **100**, 209-219.

Vignery, A. (2005). Macrophage fusion: The making of osteoclasts and giant cells. *J. Exp. Med.* **202**, 337-340.

Yagi, M., Miyamoto, T., Sawatani, Y., Iwamoto, K., Hosogane, N., Fujita, N., Morita, K., Ninomiya, K., Suzuki, T., Miyamoto, K. et al. (2005). DC-STAMP is essential for cell-cell fusion in osteoclasts and foreign body giant cells. *J. Exp. Med.* **202**, 345-351.

Yamada, S., Pokutta, S., Drees, F., Weis, W. I. and Nelson, W. J. (2005). Deconstructing the cadherin-catenin-actin complex. *Cell* **123**, 889-901.